Adaptive Neural Network Control of a Self-Balancing Two-Wheeled Scooter

Ching-Chih Tsai, *Senior Member, IEEE*, Hsu-Chih Huang, *Member, IEEE*, and Shui-Chun Lin, *Member, IEEE*

***Abstract*—This paper presents an adaptive control using radial-basis-function neural networks (RBFNNs) for a two-wheeled self-balancing scooter. A mechatronic system structure of the scooter driven by two dc motors is briefly described, and its mathematical modeling incorporating two frictions between the wheels and the motion surface is derived. By decomposing the overall system into two subsystems (yaw motion and mobile inverted pendulum), one proposes two adaptive controllers using RBFNN to achieve self-balancing and yaw control. The performance and merit of the proposed adaptive controllers are exemplified by conducting several simulations and experiments on a two-wheeled self-balancing scooter.**

***Index Terms*—Adaptive control, neural network, radial basis function, self-balancing, two-wheeled robot.**

I. Introduction

RECENTLY, self-balancing two-wheeled transporters, like the Segway, have been well recognized as powerful personal transportation vehicles. The kind of transporter can be usually constructed by a synthesis of mechatronics, control techniques, and software. For example, the Segway is made by quite high-tech and high-quality dedicated components. In contrast to the Segway, many researchers [1], [2] presented low-tech self-balancing transporters and claimed that the vehicle can be built using off-the-shelf inexpensive components. With the advent of modern technology, such transporters with sophisticated safety features can be cost down so that they, like traditional bicycles, have high potential to become prevalent two-wheeled scooters, satisfying human transportation requirements.

Design and implementation of a safe and practical self-balancing scooter is a very interesting problem. Grasser *et al.* [1] built a scaled-down prototype of a digital-signal-processor (DSP)-controlled two-wheeled vehicle based on the inverted pendulum with weights attached to it, and Pathak *et al.* [3] studied the dynamic equations of the wheeled inverted pendulum by partial feedback linearization. However, they are test prototypes, aiming at providing several theoretical design and analytical approaches. Furthermore, several researchers in [4]–[7] proposed useful control and implementation techniques for four-wheeled vehicles, two-wheeled vehicles with differential driving, and electric scooter. However, these methods cannot be directly applied to address both self-balancing and yaw control problems for the two-wheeled self-balancing scooter.

Radial-basis-function neural networks (RBFNNs) have been adopted widely for nonlinear system modeling and control because they possess simple structure, good local approximating performance, particular resolvability, and function equivalence to a simplified class of nonlinear systems [8]–[11]. Hence, RBFNNs are increasingly receiving attention in solving complex and practical problems. For examples, Li and Hori [8] presented several RBFNNs schemes for extracting fuzzy rules, and Zhuang *et al.* [9] proposed a new model for the pulsed neural network and its applications. Furthermore, Lin and Tsai [2] used two RBFNNs to approximate the unknown Coulomb and static frictions occurring in a two-wheeled self-balancing scooter; nevertheless, the method in [2] has not yet considered unmodeling errors due to linearization.

This paper contributes to the design of two adaptive controllers using RBFNNs for achieving self-balancing and yaw control. Like the JOE in [1], the proposed controllers are synthesized by decoupling this vehicle system into two subsystems: yaw motion and mobile inverted pendulum. In comparison with the state-feedback design presented by Grasser *et al.* [1], the key features of the proposed control method hinge on its mathematical modeling with Coulomb and static frictions, and its adaptive control for the scooter with unknown plant parameters, unknown frictions and linearized errors. Moreover, the proposed controllers are useful in keeping consistent driving performance for different riders, namely, that no matter what the weight of the rider is, the proposed controllers are capable of providing consistent riding performance for riders.

The three theoretical and technical contributions of this paper are given as follows. First, the two RBFNNs are employed to online approximately learn viscous and static frictions between the wheels and the motion surface, uncertainties of riders' weights, and unmodeled errors caused by linearization. Second, the proposed adaptive controllers along with parameter tuning rules are proven to be asymptotically stable via the Lyapunov stability theory. Third, the proposed controllers along with RBFNNs have been efficiently implemented by a low-cost DSP; several simulations and experimental results indicate that the proposed controllers are capable of providing appropriate control actions to steer the vehicle.

Manuscript received April 15, 2008; revised December 14, 2009. First published January 26, 2010; current version published March 10, 2010. This work was supported by the National Science Council, Taiwan, under Grants NSC 96-2221-E-005-106-MY2 and NSC 98-2218-E-241-003.

C.-C. Tsai is with the Department of Electrical Engineering, National Chung Hsing University, Taichung 402-27, Taiwan (e-mail: cctsai@nchu.edu.tw).

H.-C. Huang is with the Department of Computer Science and Information Engineering, Hung Kuang University, Taichung 433, Taiwan (e-mail: hchuang@sunrise.hk.edu.tw).

S.-C. Lin is with the Department of Electronic Engineering, National Chin-Yi University of Technology, Taichung 411, Taiwan (e-mail: lsc@ncut.edu.tw).

Color versions of one or more of the figures in this paper are available online at http://ieeexplore.ieee.org.

Digital Object Identifier 10.1109/TIE.2009.2039452

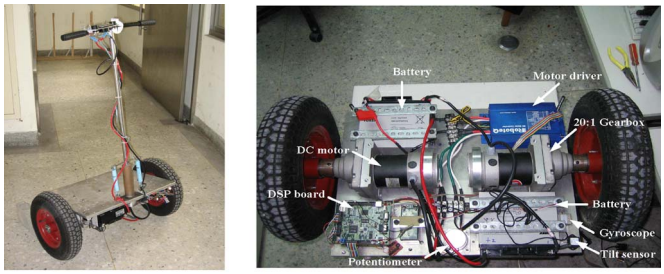

(a) (b)

Fig. 1. Laboratory-built personal two-wheeled scooter. (a) Front view (no human standing on it). (b) Bottom view.

The remainder of this paper is outlined as follows. Section II briefly describes the system design of the vehicle, and Section III shows the synthesis procedures of the two adaptive controllers using RBFNN. In Section IV, computer simulations and experimental results are presented and discussed. Section V concludes this paper.

II. System Description and Modeling

A. Mechatronic Design

Fig. 1 shows the photographs of the laboratory-based personal two-wheeled scooter with differential driving. This vehicle is composed of one footplate, two 24-V dc motors with a gearbox of ratio 20 : 1, two stamped steel wheels with 16-in tires, two 12-V sealed rechargeable lead-acid batteries in series, two motor drivers with two encoders, a single chip DSP-TMS320LF2407 from Texas Instruments as a main controller, one handle bar with a potentiometer as a position sensor, one gyroscope, and one tilt sensor. The two motor drivers use dual H-bridge circuitry to deliver pulsewidth-modulation (PWM)-based power to drive both dc motors. Sending PWM signals to the drives, the DSP outputs control signals, ranging from 0 V and 3.3 V_{DC}, to achieve self-balancing and yaw motion of the scooter. The gyroscope and the tilt sensor are employed for measuring the rate and the angle of the inclination of the footplate caused by the rider. The two rechargeable lead-acid batteries directly provide power for the two dc motors, drives, the controller and all the sensors via dc–dc buck conversion.

B. Control Architecture

Fig. 2 shows the block diagram of the scooter control system. The DSP controller with built-in A/D conversion is responsible for executing both adaptive RBFNN yaw motion and self-balancing control algorithms. The pitch rate ω_P from the gyroscope and the pitch angle θ_P from the tilt sensor are utilized via the controllers to maintain the human body on the footplate without falling. Note that both feedback signals are processed by two first-order filters, thus removing unwanted noise. The potentiometer is adopted to measure the yaw angle from the handlebar, and the yaw signal is then taken by the DSP controller for further yaw control. The output torque commands from the DSP controller are transformed into the corresponding speed commands via a torque-to-speed formula.

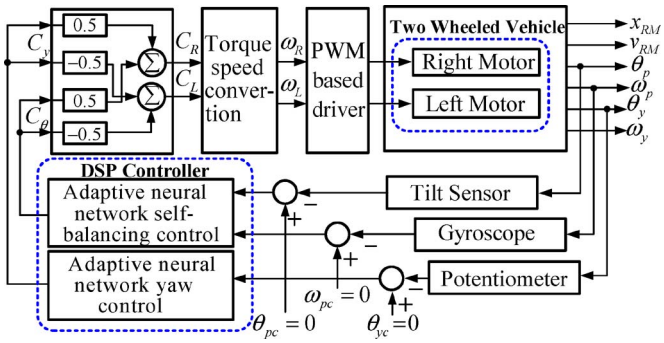

Fig. 2. Block diagram of the scooter controller.

C. Mathematical Modeling

To obtain high-performance steering experience for different riders, it is necessary to develop a mathematical model of the vehicle. The linearized mathematical model of the scooter with both viscous and static frictions is modified from [1] to [12] and given in the Appendix

$$\begin{pmatrix} \dot{x}_{RM} \\ \dot{v}_{RM} \\ \dot{\theta}_P \\ \dot{\omega}_P \\ \dot{\theta}_y \\ \dot{\omega}_y \end{pmatrix} = \begin{pmatrix} 0 & 1 & 0 & 0 & 0 & 0 \\ 0 & A_{22} & A_{23} & 0 & 0 & 0 \\ 0 & 0 & 0 & 1 & 0 & 0 \\ 0 & 0 & A_{43} & 0 & 0 & 0 \\ 0 & 0 & 0 & 0 & 0 & 1 \\ 0 & 0 & 0 & 0 & 0 & A_{66} \end{pmatrix} \begin{pmatrix} x_{RM} \\ v_{RM} \\ \theta_P \\ \omega_P \\ \theta_y \\ \omega_y \end{pmatrix} + \begin{pmatrix} 0 & 0 \\ B_2 & B_2 \\ 0 & 0 \\ B_4 & B_4 \\ 0 & 0 \\ B_6 & -B_6 \end{pmatrix} \begin{pmatrix} C_L \\ C_R \end{pmatrix} + \begin{pmatrix} 0 \\ f_2 \\ 0 \\ f_4 \\ 0 \\ f_6 \end{pmatrix}. \quad (1)$$

Similar to the vehicle, called JOE, developed by Grasser *et al.* [1], the following decoupling transformation from C_θ and C_y into the wheel torques C_R and C_L is used to decouple the system model such that both yaw motion and inverted pendulum controllers are independently designed

$$C_L = 0.5(C_\theta + C_y) \quad C_R = 0.5(C_\theta - C_y) \quad (2)$$

which converts the system (1) into two subsystems; one is the mobile inverted pendulum subsystem described by

$$\begin{pmatrix} \dot{\theta}_p \\ \dot{\omega}_p \end{pmatrix} = \begin{pmatrix} 0 & 1 \\ A_{43} & 0 \end{pmatrix} \begin{pmatrix} \theta_p \\ \omega_p \end{pmatrix} + \begin{pmatrix} 0 \\ B_4 \end{pmatrix} (C_\theta + \overline{f}_4), \quad A_{43} > 0; \quad B_4 < 0 \quad (3)$$

and the other is the yaw control subsystem described by

$$\begin{pmatrix} \dot{\theta}_y \\ \dot{\omega}_y \end{pmatrix} = \begin{pmatrix} 0 & 1 \\ 0 & A_{66} \end{pmatrix} \begin{pmatrix} \theta_y \\ \omega_y \end{pmatrix} + \begin{pmatrix} 0 \\ B_6 \end{pmatrix} (C_y + \overline{f}_6), \quad A_{66} < 0; \quad B_6 > 0 \quad (4)$$

where $\overline{f}_4 = f_4/B_4$ and $\overline{f}_6 = f_6/B_6$. Note that uncertain terms $\overline{f}_4$ and $\overline{f}_6$ account for the unmodeling errors from the linearization process, uncertainties of riders' weights, as well as the effects of disturbance forces exerted on the wheels and handle bar.

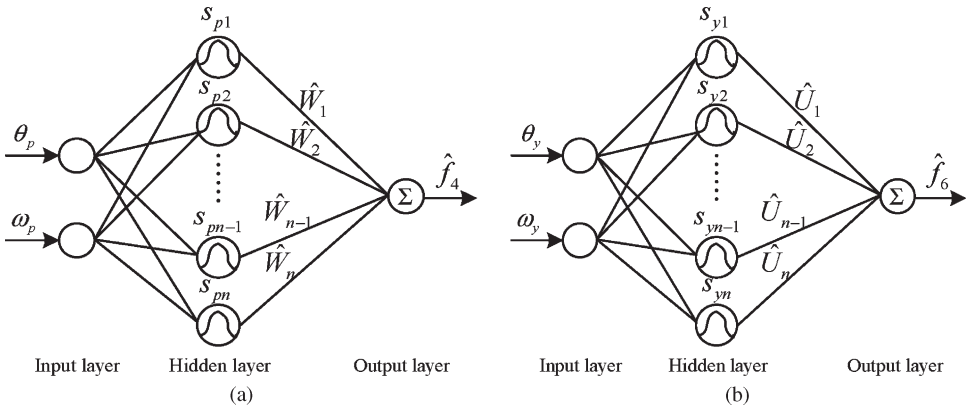

Fig. 3. (a) Structure of the RBFNN for $\overline{f}_4$. (b) Structure of the RBFNN for $\overline{f}_6$.

D. RBFNN Approximations

As shown in Fig. 3, the RBFNN performs excellent approximations for the curve-fitting problems, and it can be trained to learn some classes of nonlinear functions and system dynamics easily and quickly. One of the advantages of RBFNN is the fact that linear weights associated with the output layers can be treated separately from the hidden layer neurons. In the hidden layer, weights are adjusted through a nonlinear optimization procedure, whereas the weights of the output layer are adjusted through linear optimization. The approximation accuracy and convergent rate of the RBFNN may be further improved with a strategy for selecting appropriate centers and widths of the receptive fields. Hence, the uncertain but bounded term $\overline{f}_4$ in (3) can be approximated using the RBFNN, i.e., there exits the following function approximation:

$$|\overline{f}_4| \le \overline{f}_4^* = W^{*T} S_p^* + \varepsilon_p^* = [\, W_1^* \quad \cdots \quad W_n^* \,][\, s_{p1}^* \quad \cdots \quad s_{pn}^* \,]^{\mathrm{T}} + \varepsilon_p^* \quad (5)$$

with W^* being the optimal weight vector; ε_p^* is the bounded optimal approximation error. Moreover, the variable s_{pn} $(n = 1, 2, \ldots, 5)$ used for the RBFNN is the Gaussian function defined by

$$s_{pn}^* = \exp\left\{-\left[\left(x - u_{1pn}^*\right)^2 + \left(\dot{x} - u_{2pn}^*\right)^2\right]\sigma_{pn}^*\right\} \quad (6)$$

where u_{1pn}^* and u_{2pn}^* are the centers of the receptive field and σ_{pn}^* is the inverse of the width of the Gaussian function. Similarly, the uncertain and bounded term $\overline{f}_6$ can also be approximated by the other RBF NN over a compact set, i.e.,

$$|\overline{f}_6| \le \overline{f}_6^* = U^{*T} S_y^* + \varepsilon_y^* = [\, U_1^* \quad \cdots \quad U_n^* \,][\, s_{y1}^* \quad \cdots \quad s_{yn}^* \,]^{\mathrm{T}} + \varepsilon_y^* \quad (7)$$

where U^* denotes the optimal weight vector; ε_y^* is the bounded optimal RBFNN approximation error. Moreover, the variable s_{yn} $(n = 1, 2, \ldots, 5)$ used for the RBFNN is the Gaussian function defined by

$$s_{yn}^* = \exp\left\{-\left[\left(x - u_{1yn}^*\right)^2 + \left(\dot{x} - u_{2yn}^*\right)^2\right]\sigma_{yn}^*\right\} \quad (8)$$

where u_{1yn}^* and u_{2yn}^* are the centers of the receptive field and σ_{yn}^* is the inverse of the width of the Gaussian function.

The training inputs and output of the RBFNN for the nonlinear term $\overline{f}_4$ in the inverted wheeled pendulum subsystem (3) are θ_p, ω_p, and $\hat{f}_4$, respectively, i.e., $\hat{f}_4 = \hat{W}^{\mathrm{T}} \hat{S}_p$, where $\hat{W}$ and $\hat{S}_p$ are estimates of the optimal matrices W^* and S_p^*. Similarly, the training inputs and output of the RBFNN for the nonlinear term $\overline{f}_6$ in the yaw motion subsystem (4) are, respectively, θ_y, ω_y, and $\hat{f}_6$. Similarly, $\hat{f}_6 = \hat{U}^{\mathrm{T}} \hat{S}_y$, where $\hat{U}$ and $\hat{S}_y$ are estimates of the optimal matrices U^* and S_y^*. Note that, for the subsystem (3), the training pitch angle θ_p is taken from the tilt sensor, and its training pitch rate ω_p is directly measured from the gyroscope. For the subsystem (4), the training yaw angle θ_y and yaw rate ω_y are all from the potentiometer.

Moreover, by defining $\tilde{W} = W^* - \hat{W}$, $\tilde{S}_p = S_p^* - \hat{S}_p$, one obtains

$$\overline{f}_4^* = W^{*T} S_p^* + \varepsilon_p^* = \hat{W}^{\mathrm{T}} \hat{S}_p + \hat{W}^{\mathrm{T}} \tilde{S}_p + \tilde{W}^{\mathrm{T}} \hat{S}_p + \tilde{W}^{\mathrm{T}} \tilde{S}_p + \varepsilon_p^*. \quad (9)$$

In order to achieve online tuning of the RBFNN parameters, including the center vector $u_p = [\, u_{1p1} \quad u_{2p1} \quad u_{1p2} \quad u_{2p2} \quad \cdots \quad u_{1pn} \quad u_{2pn} \,]^{\mathrm{T}}$ and the vector $\sigma_p = [\, \sigma_{p1} \quad \sigma_{p2} \quad \sigma_{p3} \quad \cdots \quad \sigma_{pn} \,]^{\mathrm{T}}$, the expansion of $\tilde{S}_p$ is taken in a Taylor series as follows:

$$\tilde{S}_p = \frac{\partial \tilde{S}_p}{\partial \hat{u}_p}\tilde{u}_p + \frac{\partial \tilde{S}_p}{\partial \hat{\sigma}_p}\tilde{\sigma}_p + h_p = A\tilde{u}_p + B\tilde{\sigma}_p + h_p \quad (10)$$

where $\tilde{u}_p = u_p^* - \hat{u}_p$; $\tilde{\sigma}_p = \sigma_p^* - \hat{\sigma}_p$; h_p is the vector containing higher order terms and satisfies $\|h_p\| \le b_p$. Substituting (10) into (9) gives

$$\overline{f}_4^* = \hat{W}^{\mathrm{T}} \hat{S}_p + \hat{W}^{\mathrm{T}}(A\tilde{u}_p + B\tilde{\sigma}_p) + \tilde{W}^{\mathrm{T}} \hat{S}_p + \varepsilon_p \quad (11)$$

where $\varepsilon_p = \tilde{W}^{\mathrm{T}} h_p + \tilde{W}^{\mathrm{T}} \tilde{S}_p + \varepsilon_p^*$ and ε_p is assumed to satisfies $|\varepsilon_p| < g_{p\max}$.

Similarly, defining $\tilde{U} = U^* - \hat{U}$, $\tilde{S}_y = S_y^* - \hat{S}_y$ and expanding

$$\tilde{S}_y = \frac{\partial \tilde{S}_y}{\partial \hat{u}_y}\tilde{u}_y + \frac{\partial \tilde{S}_y}{\partial \hat{\sigma}_y}\tilde{\sigma}_y + h_y = C\tilde{u}_y + D\tilde{\sigma}_y + h_y \quad (12)$$

one obtains

$$\overline{f}_6^* = \hat{U}^{\mathrm{T}}\hat{S}_y + \hat{U}^{\mathrm{T}}(C\tilde{u}_y + D\tilde{\sigma}_p) + \tilde{U}^{\mathrm{T}}\hat{S}_y + \varepsilon_y \tag{13}$$

where $\tilde{u}_y = u_y^* - \hat{u}_y$; $\tilde{\sigma}_y = \sigma_y^* - \hat{\sigma}_y$; h_y is the vector including higher order terms; $\|h_y\| \le b_y$; $\varepsilon_y = \tilde{U}^{\mathrm{T}}h_y + \tilde{U}^{\mathrm{T}}\tilde{S}_y + \varepsilon_y^*$ satisfies $|\varepsilon_y| < g_{y\max}$.

III. Adaptive Control Using RBFNN

A. Adaptive Self-Balancing Controller Design Using RBFNN

This section will develop an adaptive self-balancing controller using RBFNN for the subsystem (3) with two unknown parameters A_{43} and B_4, and the uncertain term $\overline{f}_4$. The control objective is to control the angle position θ_p to reach to the command position $\theta_{pc} = 0$ without error. Due to the nonlinear term $\overline{f}_4$ in the decoupled subsystem, the well-known backstepping technique is employed in the following to accomplish the control goal. To maintain the angle position θ_p at $\theta_{pc} = 0$, one chooses the virtual control $\omega_p = -K_\theta\theta_p$, and the Lyapunov function $V_1 = \theta_p^2/2$ such that the θ_p dynamics can be stabilized at the origin. Next, one defines the subsequent backstepping error ξ_p

$$\xi_p = \omega_p + K_\theta\theta_p, \qquad K_\theta > 0 \tag{14}$$

whose time derivative becomes

$$\dot{\xi}_p = \dot{\omega}_p + K_\theta\dot{\theta}_p = A_{43}\theta_p + B_4(C_\theta + \overline{f}_4) + K_\theta\omega_p. \tag{15}$$

To stabilize the system (15), the following adaptive torque control is proposed by:

$$C_\theta = -\left[(\hat{A}_{43}+K_P)\theta_p + K_\theta\omega_p\right]\Big/\hat{B}_4 + (\hat{W}^{\mathrm{T}}\hat{S}_p + \hat{g}_p)\mathrm{sgn}(\xi_p) \tag{16}$$

where K_P and K_θ are two positive tuning parameters. With the definition of the estimation errors, $\tilde{A}_{43} = A_{43} - \hat{A}_{43}$, $\tilde{B}_4 = B_4 - \hat{B}_4$, $\tilde{g}_p = g_{p\max} - \hat{g}_p$, $\tilde{u}_p = u_p^* - \hat{u}_p$, $\tilde{\sigma}_p = \sigma_p^* - \hat{\sigma}_p$, $\tilde{W} = W^* - \hat{W}$, the parameter adaptation laws for the estimates $\hat{A}_{43}$, $\hat{B}_4$, $\hat{W}$, $\hat{g}_p$, $\hat{\sigma}_p$, and $\hat{u}_p$ are given by

$$\dot{\hat{B}}_4 = -(r_{bp}\xi_p/\hat{B}_4)\left[(K_P + \hat{A}_{43})\theta_p + K_\theta\omega_p\right]$$

$$\dot{\hat{A}}_{43} = r_{ap}\xi_p\theta_p \quad \dot{\hat{g}}_p = -r_{gp}|\xi_p| \quad \dot{\hat{u}}_p = -r_{up}A^{\mathrm{T}}\hat{W}|\xi_p|$$

$$\dot{\hat{\sigma}}_p = -r_{\sigma p}B^{\mathrm{T}}\hat{W}|\xi_p| \quad \dot{\hat{W}} = -r_{wp}\hat{S}_p|\xi_p|. \tag{17}$$

In showing (17), the substitution of (16) into the system (15) yields

$$\dot{\xi}_p = B_4\left[(\hat{W}^{\mathrm{T}}\hat{S}_p + \hat{g}_p)\mathrm{sgn}(\xi_p) + \overline{f}_4\right] - (\tilde{B}_4/\hat{B}_4)K_\theta\omega_p + \left[\tilde{A}_{43} - (\tilde{B}_4/\hat{B}_4)(K_P + \hat{A}_{43})\right]\theta_p - K_P\theta_p \tag{18}$$

and

$$\begin{aligned} d\left(\xi_p^2/2\right)/dt &= \xi_p\dot{\xi}_p \\ &\le B_4|\xi_p|\left[-\hat{W}^{\mathrm{T}}(A\tilde{u}_p + B\tilde{\omega}_p) - \tilde{W}^{\mathrm{T}}\hat{S}_p - \tilde{g}_p\right] \\ &\quad - \left[(\tilde{B}_4/\hat{B}_4)\right]K_\theta\xi_p\omega_p \\ &\quad + \left[\tilde{A}_{43} - (\tilde{B}_4/\hat{B}_4)(K_P + \hat{A}_{43})\right]\xi_p\theta_p \\ &\quad - K_P\xi_p\theta_p. \end{aligned}$$

For showing the asymptotical stability of the system, a Lyapunov function candidate is chosen by

$$\begin{aligned} V_2 &= K_P\theta_p^2/2 + \xi_p^2/2 + \tilde{A}_{43}^2/2r_{ap} + \tilde{B}_4^2/2r_{bp} \\ &\quad + B_4\tilde{W}^{\mathrm{T}}\tilde{W}/2r_{wp} + B_4\tilde{u}_p^{\mathrm{T}}\tilde{u}_p/2r_{up} \\ &\quad + \tilde{\sigma}_p^{\mathrm{T}}\tilde{\sigma}_p/2r_{\sigma p} + B_4\tilde{g}_p^2/2r_{gp} \end{aligned} \tag{19}$$

where $r_{ap} > 0$, $r_{bp} > 0$, $r_{up} < 0$, $r_{\sigma p} < 0$, $r_{wp} < 0$, $r_{gp} < 0$. Taking the time derivative of the Lyapunov candidate (19) gives

$$\begin{aligned} \dot{V}_2 \le\ & -K_PK_\theta\theta_p^2 + B_4\tilde{W}^{\mathrm{T}}\left(-\hat{S}_p|\xi_p| - \dot{\hat{W}}/r_{wp}\right) \\ & + \tilde{B}_4\left[-(K_P+\hat{A}_{43})\theta_p\xi_p/\hat{B}_4 - \dot{\hat{B}}_4/r_{bp} - K_\theta\omega_p\xi_p/\hat{B}_4\right] \\ & + \tilde{A}_{43}(\theta_p\xi_p - \dot{\hat{A}}_{43}/r_{ap}) + B_4\tilde{u}_p^{\mathrm{T}}\left(-|\xi_p|A^{\mathrm{T}}\hat{W} + \dot{\tilde{u}}_p/r_{up}\right) \\ & + \tilde{\sigma}_p^{\mathrm{T}}B_4\left(-|\xi_p|B^{\mathrm{T}}\hat{W} + \dot{\tilde{\sigma}}_p/r_{\sigma p}\right) \\ & + B_4\tilde{g}_p\left(-|\xi_p| + \dot{\tilde{g}}_p/r_{gp}\right). \end{aligned} \tag{20}$$

Clearly, if the parameter adaptation rules (17) are chosen, then $\dot{V}_2$ is negative semidefinite, i.e.,

$$\dot{V}_2 \le -K_PK_\theta\theta_p^2 \le 0. \tag{21}$$

Thus, Barbalat's lemma implies that $\theta_p \to \theta_{pc} = 0$ as $t \to \infty$. Hence, this main result is summarized as follows.

Theorem 1: Assume that $|\varepsilon_p| < g_{p\max}$, and consider the subsystem (3) with the proposed adaptive self-balancing control (16) with the parameter adjustment rules (17). Then, $\theta_p \to \theta_{pc} = 0$ as $t \to \infty$.

Remark 1: Theoretically, the pitch angle can be asymptotically stabilized at the origin, i.e., $\theta_P \to 0$ as time approaches infinity. Meanwhile, the ultimate boundedness of the Lyapunov function V_2 implies that the state variable θ_P and the backstepping error ξ_p are ultimately bounded and, from (21), ξ_p must tend to zero as $t \to \infty$. Moreover, A_{43}, B_4, ε_p, and W are also ultimately bounded, thereby obtaining the boundedness of the control signals. From (21), if both parameters K_P and K_θ are chosen larger, then the Lyapunov function V_2 quickly converges to its minimum, and, meanwhile, the state variable θ_P also quickly decays to the origin. On the other hand, once the backstepping error ξ_p have converged to zero, the state variable θ_P exponentially converges to zero since the first-order dynamic equation of θ_P is governed by $\dot{\theta}_P = -K_\theta\theta_P$.

Remark 2: K_P and K_θ are positive constants in the adaptive self-balancing controller using RBFNN. Both parameters significantly affects the regulation performance of the state variable θ_P. It is clear that the parameter K_θ is the convergent rate of the state variable θ_P via the first-order dynamic equation of θ_P, i.e., $\dot{\theta}_P = -K_\theta \theta_P$. However, saturation of the motor drives can happen if a big K_θ is used. In (21), it point outs that K_P affects the negative semidefiniteness of the derivative of the overall Lyapunov function V_2. Obviously, a larger K_P will make $\dot{V}_2$ much smaller such that V_2 quickly converges to its minimum and, meanwhile, the state variable θ_P also quickly decays to the origin.

B. Adaptive Yaw Controller Design Using RBFNN

This section is devoted to constructing an adaptive yaw controller for the subsystem (4) with the two unknown parameters, A_{66} and B_6, and the unknown nonlinear term $\overline{f}_6$. Since the potentiometer is employed to measure the angle difference between the equilibrium point and the yaw angle the rider intended to achieve, the adaptive yaw control problem is reduced to an adaptive regulation problem. Therefore, similar to the previous section, the backstepping technique is again used to attain the adaptive yaw controller by choosing the virtual control $\omega_y = -K_y\theta_y$ and the Lyapunov function $V_3 = \theta_y^2/2$, and then stabilizing the θ_y dynamics. Next, define the second backstepping error

$$\xi_y = \omega_y - (-K_y\theta_y) = \omega_y + K_y\theta_y. \tag{22}$$

Differentiating ξ_y gives

$$\dot{\xi}_y = (A_{66} + K_y)\omega_y + B_6(C_y + \overline{f}_6). \tag{23}$$

In order to stabilize the yaw control subsystem, the implicit control C_y with estimated parameters, $\hat{A}_{66}$, $\hat{B}_6$, $\hat{U}$, and $\hat{\varepsilon}_y$, is proposed as follows; for $K_{yp} > 0$ and $K_y > 0$

$$C_y = -\left[(\hat{A}_{66} + K_y)\omega_y + K_{yp}\theta_y\right] \Big/ \hat{B}_6 - (\hat{U}^{\mathrm{T}}\hat{S}_y + \hat{g}_y)\mathrm{sgn}(\xi_y). \tag{24}$$

Substituting the control law (24) into (23) gives

$$\begin{aligned}\dot{\xi}_y =& -(B_6/\hat{B}_6)K_{yp}\theta_y \\ &+ \left[\tilde{A}_{66} - (\tilde{B}_6/\hat{B}_6)(\hat{A}_{66} + K_y)\right]\omega_y \\ &+ B_6\left[-\left(\hat{U}^{\mathrm{T}}\hat{S}_y + \hat{g}_y\right)\mathrm{sgn}(\xi_y) + \overline{f}_6\right] \end{aligned}\tag{25}$$

$$\begin{aligned} d\left(\xi_y^2/2\right)/dt =& \xi_y\dot{\xi}_y \\ \le& B_6|\xi_y|\left[-\hat{U}^{\mathrm{T}}(C\tilde{u}_y + D\tilde{\sigma}_y) - \tilde{U}^{\mathrm{T}}\hat{S}_y - \tilde{g}_y\right] \\ &- (\tilde{B}_6/\hat{B}_6)K_{yp}\xi_y\theta_y \\ &+ \left[\tilde{A}_{66} - (\tilde{B}_6/\hat{B}_6)(\hat{A}_{66} + K_y)\right]\xi_y\omega_y \\ &- K_{yp}\xi_y\theta_y \end{aligned}\tag{26}$$

where $\tilde{g}_y = g_{y\max} - \hat{g}_y$. The errors of the estimated parameters are defined by $\tilde{A}_{66} = A_{66} - \hat{A}_{66}$, $\tilde{B}_6 = B_6 - \hat{B}_6$, $\tilde{U} = U^* - \hat{U}$, $\tilde{u}_y = u_y^* - \hat{u}_y$, and $\tilde{\sigma}_y = \sigma_y^* - \hat{\sigma}_y$. The following Lyapunov function candidate is employed to find the parameter updating laws:

$$\begin{aligned} V_4 =& K_{yp}\theta_y^2/2 + \xi_y^2/2 + \tilde{A}_{66}^2/2r_{ay} + \tilde{B}_6^2/2r_{by} \\ &+ B_6\tilde{U}^{\mathrm{T}}\tilde{U}/2r_{Uy} + B_6\tilde{u}_y^{\mathrm{T}}\tilde{u}_y/2r_{uy} \\ &+ B_6\tilde{\sigma}_y^{\mathrm{T}}\tilde{\sigma}_y/2r_{\sigma y} + B_6\tilde{g}_y^2/2r_{gy} \end{aligned}\tag{27}$$

where $r_{ay} > 0$, $r_{by} > 0$, $r_{Uy} > 0$, $r_{uy} > 0$, $r_{uy} > 0$, $r_{\sigma y} > 0$, $r_{gy} > 0$. Differentiating the Lyapunov function V_4 yields

$$\begin{aligned} \dot{V}_4 \le& -K_yK_{yp}\theta_y^2 + \tilde{A}_{66}(\xi_y\omega_y + \dot{\tilde{A}}_{66}/r_{ay}) \\ &+ B_6\tilde{U}^{\mathrm{T}}\left(|\xi_y|\hat{S}_y + \dot{\tilde{U}}/r_{Uy}\right) \\ &+ \tilde{B}_6\left[(-K_{yp}\xi_y\theta_y - \hat{A}_{66}\omega_y\xi_y - K_y\omega_y\xi_y)/\hat{B}_6 + \dot{\tilde{B}}_6/r_{by}\right] \\ &+ B_6\tilde{u}_y^{\mathrm{T}}\left(|\xi_y|C^{\mathrm{T}}\hat{U} + \dot{\tilde{u}}_y/r_{uy}\right) \\ &+ \tilde{\sigma}_y^{\mathrm{T}}B_6\left(|\xi_y|D^{\mathrm{T}}\hat{U} + \dot{\tilde{\sigma}}_y/r_{\sigma y}\right) + B_6\tilde{g}_y\left(|\xi_y| + \dot{\tilde{g}}_y/r_{gy}\right). \end{aligned}\tag{28}$$

If the following parameter adaptation rules are chosen:

$$\begin{aligned} \dot{\hat{B}}_6 &= (r_{by}/\hat{B}_6)(-K_{yp}\xi_y\theta_y - \hat{A}_{66}\omega_y\xi_y - K_y\omega_y\xi_y) \\ \dot{\hat{A}}_{66} &= r_{ay}\omega_y\xi_y \quad \dot{\hat{U}} = r_{Uy}S_y|\xi_y| \quad \dot{\hat{g}}_y = r_{gy}|\xi_y| \\ \dot{\hat{\sigma}}_y &= r_{\sigma y}|\xi_y|D^{\mathrm{T}}\hat{U} \quad \dot{\hat{u}}_y = r_{uy}|\xi_y|C^{\mathrm{T}}\hat{U} \end{aligned}\tag{29}$$

then, $\dot{V}_4$ becomes $\dot{V}_4 = -K_{yp}K_y\theta_y^2 \le 0$ which implies $\theta_y \to 0$ as $t \to \infty$. The following summarizes the result.

Theorem 2: Assume that $|\varepsilon_y| < g_{y\max}$, and consider the subsystem (4) with the proposed adaptive yaw control (24) with the parameter updating laws (29). Then, $\theta_y \to 0$, as $t \to \infty$.

IV. Simulations, Experiments, and Discussion

In this section, three simulations and three experiments are conducted to verify the effectiveness and performance of the proposed adaptive RBFNN self-balancing and yaw motion controllers. In all simulations and experiments, two five-node RBFNNs with online tuning of their centers and widths are used to approximately learn these two uncertain but bounded terms, $\overline{f}_4$ and $\overline{f}_6$.

The first simulation is conducted to verify the performance of the proposed adaptive RBFNN self-balancing controller. Fig. 4 shows the comparison of the simulation results of the pitch angle tracking for the state-feedback controller [1] and the adaptive controller using RBFNN. As shown in Fig. 4, the adaptive self-balancing controller using RBFNN has a faster convergent speed than the state-feedback controller does. The second simulation is performed to examine the effectiveness of the proposed adaptive RBFNN yaw motion controller. Fig. 5 shows the yaw angle tracking performance for the

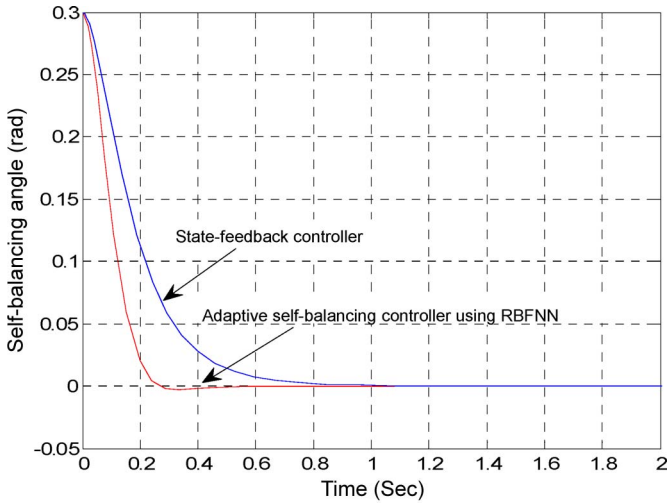

Fig. 4. Comparison of simulation results of the pitch angle tracking for the state-feedback controller [1] and the adaptive self-balancing controller using RBFNN.

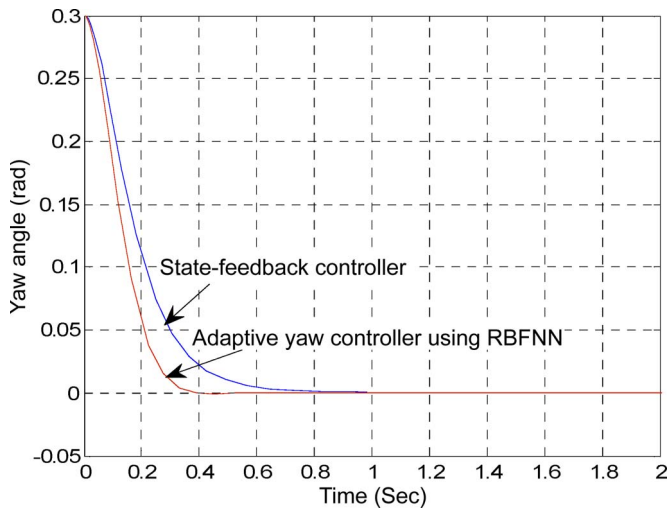

Fig. 5. Comparison of simulation results of the yaw angle tracking for the state-feedback controller [1] and the adaptive yaw controller using RBFNN.

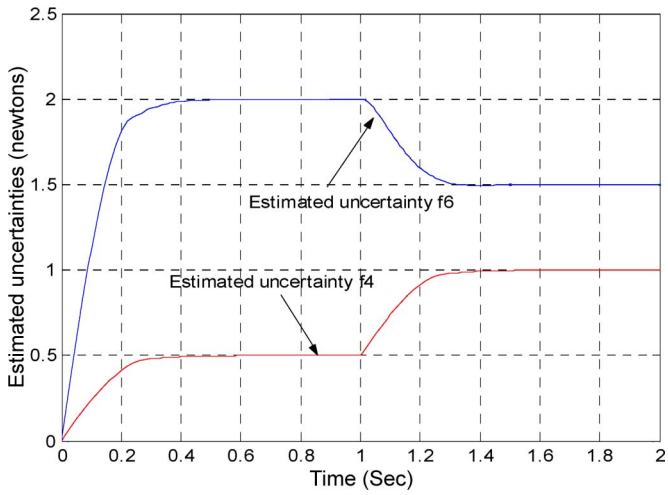

Fig. 6. RBFNN approximations of $\hat{f}_4 = \hat{W}^{\mathrm{T}}\hat{S}_p$ and $\hat{f}_6 = \hat{U}^{\mathrm{T}}\hat{S}_y$.

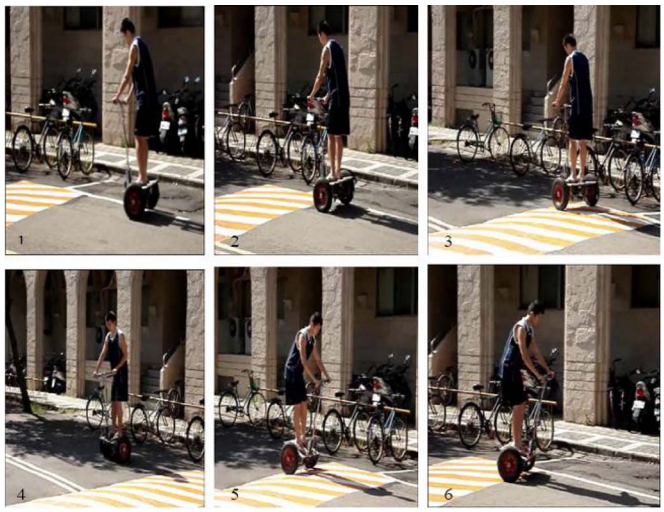

Fig. 7. Sequential still images captured from the experimental video for the self-balancing two-wheeled scooter.

state-feedback controller and the proposed yaw controller using RBFNN. The results in Fig. 5 clearly indicate that the proposed adaptive yaw controller with RBFNN has a better response than the conventional state-feedback controller does. The results in Figs. 4 and 5 have shown that the proposed controller outperforms the state-feedback controller.

In addition, the third simulation is conducted to investigate the learning performance of both RBFNNs. These uncertain terms, f_4 and f_6, use nonconstant static frictions varying with different terrains, and unmodeled errors between the nonlinear model and the linearized model adopted in this paper, but neglects the viscous frictions depending upon the vehicle speed. The nonlinear uncertainties f_4 and f_6 are, respectively, given by

$$f_4 = \begin{cases} 0.5\,\mathrm{N} + n(t), & 0\,\mathrm{s} < t < 1\,\mathrm{s} \\ 1\,\mathrm{N} + n(t), & t > 1\,\mathrm{s} \end{cases}$$

$$f_6 = \begin{cases} 2\,\mathrm{N} + n(t), & 0\,\mathrm{s} < t < 1\,\mathrm{s} \\ 1.5\,\mathrm{N} + n(t), & t > 1\,\mathrm{s} \end{cases}$$

where $n(t)$ is a white Gaussian process with zero mean and variance of 0.1.

Fig. 6 shows that the nonlinear uncertainty f_4 and f_6 can be well approximated by the output of the RBFNNs, i.e., $\hat{f}_4 = \hat{W}^{\mathrm{T}}\hat{S}_p$ and $\hat{f}_6 = \hat{U}^{\mathrm{T}}\hat{S}_y$. The results, in both cases, have confirmed that the two nonlinear uncertainties can be well approximated by the two RBFNNs.

The subsequent experiments studied that the rider can easily steer the designed scooter. Fig. 7 shows the sequential still images captured from the experimental video for the self-balancing two-wheeled scooter. Figs. 8 and 9 show the experimental results of the two proposed controllers with RBFNNs. These results have exemplified the effectiveness of the proposed controller for self-balancing of the two-wheeled scooter. As shown in Figs. 8 and 9, both experimental results are in good agreement with simulation ones. As mentioned in Section II, the two first-order low-pass filters are used to eliminate high-frequency noise in the pitch and yaw motion responses, thus retaining the dynamics of the proposed controller.

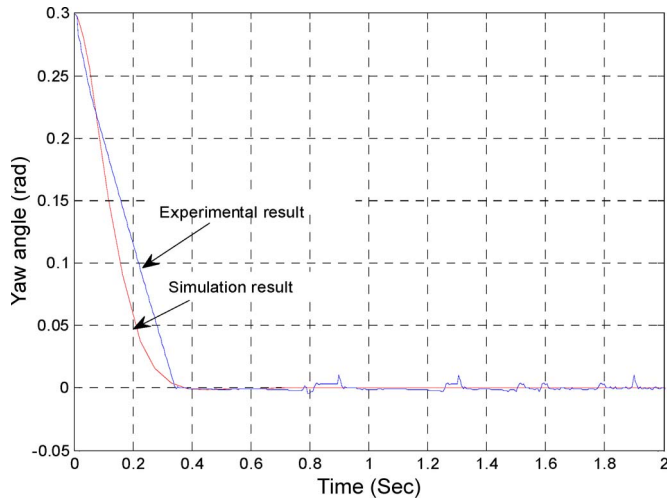

Fig. 8. Experimental yaw response of the adaptive yaw controller using RBFNN.

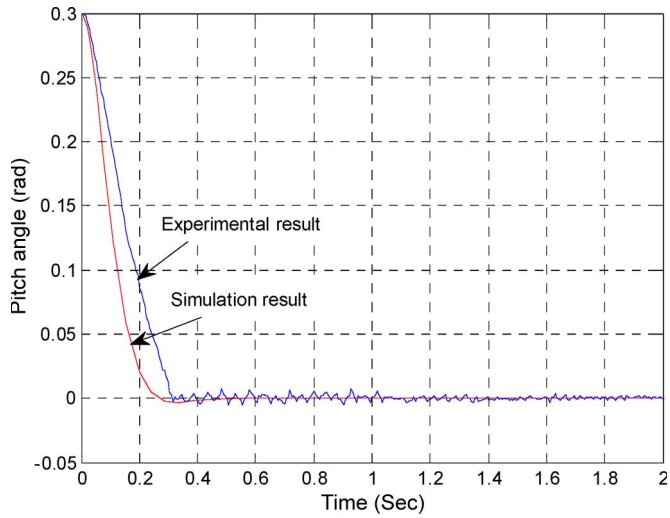

Fig. 9. Experimental pitch response of the adaptive self-balancing controller using RBFNN.

V. Conclusion

This paper has presented an adaptive control using RBFNN for a self-balancing two-wheeled scooter. The mechatronic method has been successfully used to construct the vehicle, and the linearized mathematical modeling of the vehicle with two unknown frictions has been well established in a state-space framework. With the decomposition of the system into its two subsystems, two adaptive controllers using RBFNN have been synthesized to achieve self-balancing and desired yaw motion. Through simulations and experimental results, the proposed controllers have been shown useful and effective in providing appropriate control actions to steer the vehicle at slow speeds. An important topic for future research would be to develop an adaptive fuzzy controller for the scooter running at high speeds.

Appendix

This appendix will briefly describe how to establish a mathematical model of the experimental scooter with the definitions of parameters in Table I.

TABLE I
Definitions of Parameters

x_{RM}, v_{RM}	Position, speed
θ_P, ω_P	Pitch angle, pitch angle rate
θ_y, ω_y	Yaw angle, yaw angle rate
C_L	Applied torque on the left wheel
C_R	Applied torque on the right wheel
J_{RL}, J_{RR}	Moment of inertia of the left and right wheels; $J_{RL}=J_{RR}$
M_{RR}, M_{RL}	Mass of the left and right wheel; $M_{RR}=M_{RL}$
$J_{p\theta}$	Moment of inertia of the chassis with respect to the z axis
J_{py}	Moment of inertia of the chassis with respect to the y axis
M_P	Mass of the chassis with the weight of the rider
R	Radius of the wheels
D	Lateral distance between the contact patches of the wheels
L	Distance between the z axis and the center of gravity of the chassis
b	Viscous friction coefficient for both wheels
f_c	Static friction coefficient for both wheels
$v_{RL}(v_{RR})$	Linear speed of the left (right) wheel
$\omega_{RL}(\omega_{RR})$	Angular velocity of the left (right) wheel
$\theta_{RL}(\theta_{RR})$	Shaft angle of the left (right) wheel
$\omega_{RPL}(\omega_{RPR})$	Angular velocity of the left (right) wheel
$\theta_{RPL}(\theta_{RPR})$	Shaft angle of the left (right) wheel
$f_{dRL}(f_{dRR})$	Forces applied to the center of the left (right) wheels
f_{dp}	Forces applied to the center of gravity

The nonlinear dynamic system model of the experimental scooter is described by the following set of motion equations via Newtonian mechanism [1], [12]. Three equations of the right wheel for translation and rotation are governed by

$$M_{RR}\ddot{x}_{RR} = f_{dRR} + H_{TR} - H_R - b\dot{x}_{RR} - f_c\mathrm{sgn}(\dot{x}_{RR}) \tag{A.1}$$

$$M_{RR}\ddot{y}_{RR} = V_{TR} - M_{RR}g - V_R \tag{A.2}$$

$$J_{RR}\ddot{\theta}_{RR} = C_R - (H_{TR} - b\dot{x}_{RR} - f_c\mathrm{sgn}(\dot{x}_{RR}))\,R. \tag{A.3}$$

Similarly, three equations of motion for the left wheel are governed by

$$M_{RL}\ddot{x}_{RL} = f_{dRL} + H_{TL} - H_L - b\dot{x}_{RL} - f_c\mathrm{sgn}(\dot{x}_{RL}) \tag{A.4}$$

$$M_{RL}\ddot{y}_{RL} = V_{TL} - M_{RL}g - V_L \tag{A.5}$$

$$J_{RL}\ddot{\theta}_{RL} = C_L - (H_{TL} - b\dot{x}_{RL} - f_c\mathrm{sgn}(\dot{x}_{RL}))\,R \tag{A.6}$$

where the forces H_{TR}, H_R, V_{TR}, V_R, H_{TL}, H_L, V_{TL}, and V_L are defined in [1]. Furthermore, the equations of motion of the

chassis for translation in both horizontal and vertical directions, and rotation are expressed by

$$M_P\ddot{x}_P = f_{dP} + H_R + H_L \tag{A.7}$$

$$M_p\ddot{y}_p = V_R + V_L - M_p g \tag{A.8}$$

$$J_{p\theta}\ddot{\theta}_P = (V_R + V_L)L\sin\theta_p - (H_R + H_L)L\cos\theta_p - (C_L + C_R). \tag{A.9}$$

Assume that θ_P be small, i.e., $y_P = L\cos\theta_P \approx L$, $\ddot{y}_p = 0$. Using the linearization procedure, one defines the following six state variables:

$$\mathbf{X} = [x_{RM} \quad v_{RM} \quad \theta_P \quad \omega_P \quad \theta_y \quad \omega_y]^{\mathrm{T}}.$$

After lengthy algebraic manipulations [10], one obtains the linearized system model of the scooter in the following state-space form:

$$\begin{bmatrix} \dot{\boldsymbol{\mathcal{X}}}_{RM} \\ \dot{v}_{RM} \\ \dot{\theta}_P \\ \dot{\omega}_p \\ \dot{\theta}_y \\ \dot{\omega}_y \end{bmatrix} = \begin{bmatrix} 0 & 1 & 0 & 0 & 0 & 0 \\ 0 & A_{22} & A_{23} & 0 & 0 & 0 \\ 0 & 0 & 0 & 1 & 0 & 0 \\ 0 & 0 & A_{43} & 0 & 0 & 0 \\ 0 & 0 & 0 & 0 & 0 & 1 \\ 0 & 0 & 0 & 0 & 0 & A_{66} \end{bmatrix} \begin{bmatrix} \boldsymbol{\mathcal{X}}_{RM} \\ v_{RM} \\ \theta_P \\ \omega_p \\ \theta_y \\ \omega_y \end{bmatrix} + \begin{bmatrix} 0 & 0 & 0 & 0 & 0 \\ B_{21} & B_{22} & B_{23} & B_{24} & B_{25} \\ 0 & 0 & 0 & 0 & 0 \\ B_{41} & B_{42} & 0 & 0 & B_{45} \\ 0 & 0 & 0 & 0 & 0 \\ B_{61} & B_{62} & B_{63} & B_{64} & 0 \end{bmatrix} \begin{bmatrix} C_L \\ C_R \\ f_{dRL} \\ f_{dRR} \\ f_{dP} \end{bmatrix} + \begin{pmatrix} 0 \\ \xi_2 \\ 0 \\ \xi_4 \\ 0 \\ \xi_6 \end{pmatrix} \tag{A.10}$$

where ξ_i $(i = 2, 4, 6)$, respectively, denotes the uncertain term which may include static frictions and linearized errors. Furthermore, let $\alpha = (M_R R^2/J_{RR}) + 1$, $\beta = (J_{P\theta}/M_P L) + L$, $p = 1 + D^2(J_{RR} + M_{RR}R^2)/2J_{py}R^2$, then the system parameters in (A.10) are given by

$$A_{22} = (-R^2/J_{RR})(b/\alpha) \quad A_{23} = -(R^2/2J_{RR})(\gamma/\alpha\beta)$$

$$B_{21} = B_{22} = R/2J_{RR}\left[(1/\alpha) + (R/\alpha\beta)\right]$$

$$B_{23} = B_{24} = R^2/2J_{RR}\alpha$$

$$B_{25} = (R^2/2J_{RR})(1/\alpha\beta)(J_{P\theta}/M_P L)$$

$$A_{43} = (\gamma/J_{P\theta})(1 - L/\beta)$$

$$B_{41} = B_{42} = (1/J_{P\theta})\left((L/\beta) - 1\right) \quad B_{45} = 1/\beta M_p$$

$$A_{66} = -(D^2 b + 2b)/(2J_{Py})$$

$$B_{61} = -B_{62} = D/2J_{Py}R \quad B_{63} = -B_{64} = D/2J_{Py}.$$

From (A.10), if the scooter without uncertainties has a steady-state tilt angle, then it will provide a steady-state linear speed $v_{RM_{\mathrm{SS}}}$ $(v_{RM_{\mathrm{SS}}} = ((B_2A_{43} - A_{23}B_6)/A_{22}B_6)\theta_p)$ to make the scooter move without falling down. Moreover, (A.10) can be simply rewritten by

$$\begin{pmatrix} \dot{x}_{RM} \\ \dot{v}_{RM} \\ \dot{\theta}_P \\ \dot{\omega}_P \\ \dot{\theta}_y \\ \dot{\omega}_y \end{pmatrix} = \begin{pmatrix} 0 & 1 & 0 & 0 & 0 & 0 \\ 0 & A_{22} & A_{23} & 0 & 0 & 0 \\ 0 & 0 & 0 & 1 & 0 & 0 \\ 0 & 0 & A_{43} & 0 & 0 & 0 \\ 0 & 0 & 0 & 0 & 0 & 1 \\ 0 & 0 & 0 & 0 & 0 & A_{66} \end{pmatrix} \begin{pmatrix} x_{RM} \\ v_{RM} \\ \theta_P \\ \omega_P \\ \theta_y \\ \omega_y \end{pmatrix} + \begin{pmatrix} 0 & 0 \\ B_2 & B_2 \\ 0 & 0 \\ B_4 & B_4 \\ 0 & 0 \\ B_6 & -B_6 \end{pmatrix} \begin{pmatrix} C_L \\ C_R \end{pmatrix} + \begin{pmatrix} 0 \\ f_2 \\ 0 \\ f_4 \\ 0 \\ f_6 \end{pmatrix} \tag{A.11}$$

where $B_2 = B_{21} = B_{22}$, $B_4 = B_{41} = B_{42}$, $B_6 = B_{61} = B_{62}$. Moreover, the three uncertainties, f_2, f_4 and f_6, can be realistically modeled by

$$\begin{aligned} f_2 &= B_{23}f_{dRL} + B_{24}f_{dRR} + B_{25}f_{dP} + \xi_2 \\ f_4 &= B_{45}f_{dP} + \xi_4 \\ f_6 &= B_{63}f_{dRL} + B_{64}f_{dRR} + \xi_6. \end{aligned} \tag{A.12}$$

REFERENCES

[1] F. Grasser, A. D. Arrigo, and S. Colombi, "JOE: A mobile, inverted pendulum," *IEEE Trans. Ind. Electron.*, vol. 49, no. 1, pp. 107–114, Feb. 2002.

[2] S. C. Lin and C. C. Tsai, "Development of a self-balancing human transportation vehicle for the teaching of feedback control," *IEEE Trans. Educ.*, vol. 52, no. 1, pp. 157–168, Feb. 2009.

[3] K. Pathak, J. Franch, and S. K. Agrawal, "Velocity and position control of a wheeled inverted pendulum by partial feedback linearization," *IEEE Trans. Robot. Autom.*, vol. 21, no. 3, pp. 505–513, Jun. 2005.

[4] H. Ohara and T. Murakami, "A stability control by active angle control of front-wheel in a vehicle system," *IEEE Trans. Ind. Electron.*, vol. 55, no. 3, pp. 1277–1285, Mar. 2008.

[5] I. Baturone, F. J. Moreno-Velo, V. Blanco, and J. Ferruz, "Design of embedded DSP-based fuzzy controllers for autonomous mobile robots," *IEEE Trans. Ind. Electron.*, vol. 55, no. 2, pp. 928–936, Feb. 2008.

[6] C. H. Chen and M. Y. Cheng, "Implementation of a highly reliable hybrid electric scooter drive," *IEEE Trans. Ind. Electron.*, vol. 54, no. 5, pp. 2462–2473, Oct. 2007.

[7] N. Mutoh, Y. Hayano, H. Yahagi, and K. Takita, "Electric braking control methods for electric vehicles with independently driven front and rear wheels," *IEEE Trans. Ind. Electron.*, vol. 54, no. 2, pp. 1168–1176, Apr. 2007.

[8] W. Li and Y. Hori, "An algorithm for extracting fuzzy rules based on RBF neural network," *IEEE Trans. Ind. Electron.*, vol. 53, no. 4, pp. 1269–1276, Aug. 2006.

[9] H. Zhuang, K. S. Low, and W. Y. Yau, "A pulsed neural network with on-chip learning and its practical applications," *IEEE Trans. Ind. Electron.*, vol. 54, no. 1, pp. 34–42, Feb. 2007.

[10] M. A. M. Radzi and N. A. Rahim, "Neural network and bandless hysteresis approach to control switched capacitor active power filter for reduction of harmonics," *IEEE Trans. Ind. Electron.*, vol. 56, no. 5, pp. 1477–1484, May 2009.

[11] S. Cong and Y. Liang, "PID-like neural network nonlinear adaptive control for uncertain multivariable motion control system," *IEEE Trans. Ind. Electron.*, vol. 56, no. 10, pp. 3872–3879, Oct. 2009.

[12] S. C. Lin, "System design, modeling and control of self-balancing human transportation vehicles," Ph.D. dissertation, Dept. Elect. Eng., Nat. Chung Hsing Univ., Taichung, Taiwan, Jul. 2008.

Ching-Chih Tsai (S'90–M'92–SM'00) received the Diplomat in electrical engineering from National Taipei Institute of Technology, Taipei, Taiwan, in 1981, the M.S. degree in control engineering from National Chiao Tung University, Hsinchu, Taiwan, in 1986, and the Ph.D. degree in electrical engineering from Northwestern University, Evanston, IL, in 1991.

He is currently a Distinguished Professor in the Department of Electrical Engineering, National Chung Hsing University, Taichung, Taiwan, where he served as the Director of the Center for Research Development and Engineering Technology, College of Engineering, from 2003 to 2005, and the Director of the Center for Advanced Industry Technology and Precision Processing in 2006. He has published and coauthored over 280 technical papers. His current research interests include ultrasonics, mechatronics, mobile robotics, advanced control methods (predictive control, adaptive control, nonlinear control, and intelligent control), embedded control systems, and their applications to mobile robots and industrial control systems.

Dr. Tsai is a Fellow of the Institute of Enginnering Technology and of the Chinese Automatic Control Society, Taiwan. He served as the Chair of the IEEE Control Systems Society, Taipei Chapter, from 2001 to 2003, and the Chair of the IEEE Robotics and Automation Society, Taipei Chapter, in 2006. He has been the President of the Chinese Institute of Engineers, Taiwan, Taichung Chapter, since 2007, and the Chair of the IEEE Systems, Man, and Cybernetics Society, Taichung Chapter, since 2009.

Hsu-Chih Huang (S'08–M'09) received the M.S. degree from the Institute of Biomedical Engineering, National Cheng Kung University, Tainan, Taiwan, in 1999, and the Ph.D. degree in electrical engineering from National Chung Hsing University, Taichung, Taiwan, in 2008.

He is currently an Assistant Professor in the Department of Computer Science and Information Engineering, Hung Kuang University, Taichung. His current research interests include intelligent control, mobile robots, embedded systems, system on a programmable chip, and nonlinear control.

Shui-Chun Lin (S'06–M'09) received the B.S. degree in electronic engineering from National Taiwan University of Science and Technology, Taipei, Taiwan, in 1988, and the M.S. and Ph.D. degrees in electrical engineering from National Chung Hsing University, Taichung, Taiwan, in 2002 and 2008, respectively.

He is currently an Associate Professor in the Department of Electronic Engineering, National Chin-Yi University of Technology, Taichung. His current research interests include nonlinear control, adaptive control, sliding-mode control, and their applications to power electronics and industrial systems.